HHS Public Access

Author manuscript

J Chem Inf Model. Author manuscript; available in PMC 2021 July 14.

Published in final edited form as:

J Chem Inf Model. 2020 May 26; 60(5): 2644–2650. doi:10.1021/acs.jcim.0c00010.

Cylindrical Similarity Measurement for Helices in Medium-Resolution Cryo-Electron Microscopy Density Maps

Salim Sazzed, **Peter Scheible**, **Maytha Alshammari**

Department of Computer Science, Old Dominion University, Norfolk, Virginia 23529, United States

Willy Wriggers,

Department of Mechanical and Aerospace Engineering, Old Dominion University, Norfolk, Virginia 23529, United States

Jing He

Department of Computer Science, Old Dominion University, Norfolk, Virginia 23529, United States

Abstract

Cryo-electron microscopy (cryo-EM) density maps at medium resolution (5–10 Å) reveal secondary structural features such as α-helices and β-sheets, but they lack the side chain details that would enable a direct structure determination. Among the more than 800 entries in the Electron Microscopy Data Bank (EMDB) of medium-resolution density maps that are associated with atomic models, a wide variety of similarities can be observed between maps and models. To validate such atomic models and to classify structural features, a local similarity criterion, the F_1 score, is proposed and evaluated in this study. The F_1 score is theoretically normalized to a range from zero to one, providing a local measure of cylindrical agreement between the density and atomic model of a helix. A systematic scan of 30,994 helices (among 3,247 protein chains modeled into medium-resolution density maps) reveals an actual range of observed F_1 scores from 0.171 to 0.848, suggesting that the cylindrical fit of the current data is well stratified by the proposed measure. The best (highest) F_1 scores tend to be associated with regions that exhibit high and spatially homogeneous local resolution (between 5 Å and 7.5 Å) in the helical density. The proposed F_1 scores can be used as a discriminative classifier for validation studies and as a ranking criterion for cryo-EM density features in databases.

Graphical Abstract

Corresponding Author: Jing He – *Department of Computer Science, Old Dominion University, Norfolk, Virginia 23529, United States;* jhe@cs.odu.edu.

Author Contributions

S.S. and J.H. developed the F_1 score method, and S.S. and P.S. implemented it. P.S. and M.A. carried out the analysis of the large data set. J.H. and W.W. wrote the manuscript. J.H. supervised the project.

The authors declare no competing financial interest.

Complete contact information is available at: https://pubs.acs.org/10.1021/acs.jcim.0c00010

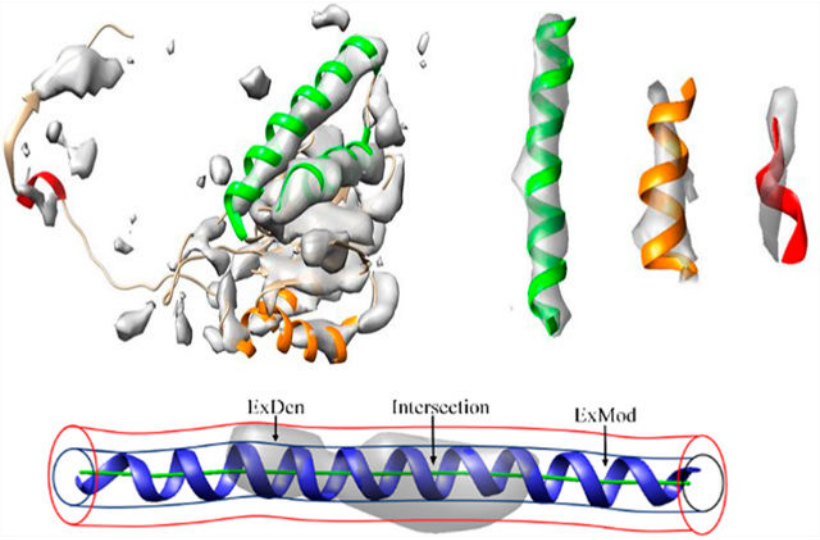

INTRODUCTION

The number of atomic structures that are derived from cryo-electron microscopy (cryo-EM) density maps has increased rapidly over the last five years. As of December 1, 2019, there were 824 structures modeled from cryo-EM density maps at reported resolution values in the medium- resolution range (5–10 Å) compared to 3,144 structures derived from resolutions better than 5 Å.[1,2] It is, of course, desirable to obtain high-resolution maps (better than 3.4 Å resolution is typically required to directly solve atomic structures). The quality of a map produced by an experimental cryo-EM laboratory improves over time as more data is collected. Consequently, medium-resolution maps are routinely created in the initial stages of a cryo-EM imaging project, before the specimen preparation protocols are tuned to perfection. Lower-resolution regions can also be present in overall high-resolution maps due to conformational flexibility or libration of the specimen. For these reasons, medium-resolution maps are often the first and only observations available of a new system. Such early glimpses of an unknown system can be of significant biological importance, and there is pressure to interpret them at atomic detail. Understandably, investigators will attempt to build models despite the risks and inaccuracies. Our present work is concerned with assessing the accuracy of the model fit given the increasing number of deposited map/model pairs in the challenging medium-resolution range.

Various structural modeling methods have been developed to utilize known atomic structures as initial templates. Some structures were derived from medium-resolution density maps through rigid-body fitting[3,4] and real space refinement.[5–8] Other structures were derived using comparative modeling methods[9–13] and flexible fitting.[14–18] It remains quite difficult and risky to model atomic structures *de novo* for most proteins, owing to the resolution limitations. However, in many cases, secondary structure elements, such as α-helices and β-sheets, can be assigned with confidence into medium-resolution maps.[19–26] Our understanding of the quality of density patterns and corresponding atomic models in medium-resolution maps is limited. Without knowledge of reliable density patterns, it is

risky to overfit atomic models on erroneous density or to underutilize reliable density patterns in model building.

Among secondary structural features, α-helices often appear as cylindrically shaped density regions, and β-sheets appear as thin layers of density in medium-resolution cryo-EM maps. Although the location of α-helices is commonly detectable,[21,22,24,25] density strength varies considerably at helix regions.[27] The density of some helices appears to fill almost all of the helix backbone region expected of the atomic structure (green helices in Figure 1) when visualized at a threshold tuned to the surface of secondary structural features. Other helix backbone regions appear to be partially filled (orange helices in Figure 1); but for some outliers, the orientation of the helix appears to be different from the direction of the corresponding density region (red helix in Figure 1). Variations in density strength can be explained by the limitations of systematic image processing, such as image alignment and 3D reconstruction artifacts, or structural flexibility of molecules. To represent a spatially heterogeneous level of detail[28,29] that is often observed in cryo-EM maps, the concept of local resolution has recently been introduced. While local resolution provides important information about the quality of specific regions of a map, it is not clear how the concept can be best utilized in model building. Due to the effects of noise, density sharpening, correction of microscope parameters, and 3D reconstruction, individual voxels may not be reliable; moreover, the voxel spacing is typically much finer than indicated by the medium-spatial resolution.

In this work, we therefore propose to assess the local quality of a map at the level of secondary structure elements. The level of detail of a similarity measure based on secondary structure elements, such as helices, is, by design, intermediate between individual voxels and the global map. The features are large enough to be robust, but the similarity measure is still a local one, compared to the global cross-correlation coefficient.[30]

The reproducibility and discriminative ability of a local similarity score is important during the model-building process, because a global score, such as the cross-correlation (CC), varies with the size of the map volume under consideration. Consequently, an earlier application of CC scores in the *PHENIX* program required a local region mask[31] to evaluate individual residues. An alternative tool, *EM-Ringer*, evaluated side chains only and produced a single score to represent the quality of the fit, but the approach did not generalize to the secondary structure level.[32] The closest related approach, in terms of applicability to a secondary structure, was the Z-score.[33] A Z-score was calculated from 27 CC scores using ± zero or one voxel shifts in the x, y, and z directions, respectively.[33] The approach did not take specific shape information into account, and by design it depended on the granularity of the map. In contrast, the new F_1 score proposed below uses a simple geometric metric and is invariant when zooming in to the level of residues.

Despite the challenges associated with interpreting medium-resolution density maps, over 800 atomic models have already been derived from such data, mostly through fitting an existing X-ray structure followed by refinement. Since each atomic model often involves multiple chains, and each chain, in turn, often has multiple helices and β-sheets, the large number of map/model pairs provides a solid data set for a quantitative analysis. Since helices

are the more distinctive secondary structural feature and visible across the entire medium-resolution range, this study proposes a quantitative score to evaluate cylindrical similarity for helix regions in a medium-resolution density map. Owing to the diverse 3D reconstruction and modeling approaches used in cryo-EM and a resulting multitude of potential algorithmic and experimental limitations, the similarity score was designed to be agnostic of the origin of a specific mismatch (the unaccounted for regions ExMod or ExDen in Figure 2C).

METHODOLOGY

Data.

On September 9, 2018, we downloaded 654 medium-resolution cryo-EM density maps with corresponding atomic models from the EMDB and PDB, respectively. For a protein with multiple copies of the same chain sequence, only one was included to eliminate redundancies. The final data set consisted of 3,247 protein chains. The cryo-EM density region corresponding to each chain was extracted from the entire density map using *UCSF Chimera* with a radius of 5 Å around each atom.[3] Because the method was designed to measure helices, chains without helices were excluded. Chains that lay completely outside any molecular density were also excluded.

Cylindrical Similarity Score.

The density distribution of a helix closely resembles a cylinder at medium resolution, with highest densities found near the central axis of the helix. The similarity of an atomic model was quantified using two suitably chosen template cylinders, derived from the central line of a helix using Cα atoms (Figure 2C). The central line was produced using the *AxisComparison* tool from an atomic model in PDB format.[34,35] In the *AxisComparison* method, every four consecutive Cα atoms of a helix are averaged to generate initial central points, which are interpolated to produce a smooth line (Figure 2C). The radius was selected as 2.5 and 4 Å for the inner and outer cylinders, respectively, to approximate the radius of the helix backbone and a typical radial size of an α-helix. We also explored 3 and 5 Å for inner and outer cylinder radii, respectively, but we found that the use of 4 Å radius for the outer cylinder reduced the density overlap from surrounding nonhelix density. At each density threshold, the number of helix density voxels within the inner cylinder, *VxInner*, measured the (ideally large) volume of the intersection between the helix density and the model (Figure 2C). The number of helix density voxels between the inner and outer cylinder, *VxOut*, measured the (ideally small) volume of identifiable helix voxels outside of the helix backbone model (denoted ExDen in Figure 2C). The number of inner cylinder voxels that have lower densities than the threshold, $\overline{VxInner}$, measured the (ideally small) volume where the atomic helix backbone model was not supported by sufficient map density (denoted ExMod in Figure 2C). Both *VxOut* and $\overline{VxInner}$ lowered the F_1 score via eqs 1–3.

$$F_1 = \frac{2*Pden*Rmod}{Pden+Rmod} \quad (1)$$

$$Pden = \frac{Intersection}{Intersection + ExDen} = \frac{VxInner}{VxInner + VxOut} \quad (2)$$

$$Rmod = \frac{Intersection}{Intersection + Exmod} = \frac{VxInner}{VxInner + \overline{VxInner}} \quad (3)$$

Density thresholds were sampled between the mean and the maximum of the density map, and the threshold that maximized the F_1 score (eq 1) was selected automatically.

The F_1 score is a metric commonly used in machine learning. Our adaptation of the F_1 score (eq 1) was adapted from the standard interpretation in statistics where the F_1 score is the harmonic mean of precision and recall.[36] Although it is typically used to compare ground truth and prediction, the F_1 score in our implementation measured similarity between two sets: the density region (above a threshold) in the vicinity of a helix and the region of a helix backbone model. *Pden* (eq 2) represents the accuracy of the helix density, i.e., the percentage of agreed map/model volume among the total volume of map relevant to the helix. *Rmod* (eq 3) represents the accuracy of the model, i.e., the percentage of agreed map/model volume among the total volume relevant to the helix backbone model. F_1 scores lie between zero and one, where one indicates perfect similarity between the two sets.

RESULTS

When the resolution is high, such as at about 4 Å, the coil of the helix backbone starts to become visible in cryo-EM density maps (Figure 2A): the helix backbone exhibits a higher density than the side chains. The higher density of the helix backbone thus requires a density threshold for visualization that obscures the expected side chain regions (Figure 2A). At medium resolution, however, instead of the coil of the backbone, only a cylindrically shaped density is observed (Figure 2B): the highest density voxels are often located near the central axis of the cylinder. We used two cylinders to measure the cylindrical character of the density along a helix that is represented by the central axis of a helix atomic model. The inner radius of 2.5 Å was designed to capture the backbone density of a helix: a helix with good map/model similarity is expected to have a density threshold at which the density is primarily located within the inner cylinder of 2.5 Å radius.

The cylindrical similarity of helices was evaluated for 30,994 helices from 3,247 protein chains corresponding to maps with resolutions between 5 Å and 10 Å. Each helix region in Figure 3 was shown using the automatically selected density threshold that maximizes the F_1 score. The observed F_1 scores varied considerably, and those helices with higher F_1 scores appear more cylindrical through the entire length of the model. The F_1 score also appears to stratify the data as intended. As an example, the helix located on chain D of PDB ID 5j4z between amino acid segment 131 to 161 appeared to have a good cylindrical shape (top left in Figure 3). The maximum F_1 score of the helix was 0.863 when the density threshold was at 0.159, at which the inner cylinder was maximally filled, while the density volume between inner and outer cylinder was minimized.

When a helix was not clearly distinguishable from the surrounding density in some spots, such as in EMDB ID 3536 chain P segment 334–356 (middle of the second row in Figure 3), *Pden* was lower since the indistinguishable density was reflected in *VxOut*. In this case, the accuracy of the helix density was 0.613, and the F_1 score was 0.698 (Table 1). When a misalignment occurred between helix density and its atomic model, such as in the helix in EMDB ID 3164 chain V from amino acid 29 to 47 (first example in the bottom row in Figure 3), the shifted density contributed to reduced *VxInner* and increased *VxOut*. The resulting F_1 score was 0.618 in this case (Table 1).

The histogram of helix F_1 scores shows that the most frequent F_1 scores were at about 0.55 with about 1,600 helices (Figure 4A). Populations with F_1 scores less than 0.55 sharply reduced as the score decreased. Three examples with F_1 scores lower than 0.55 show a poor match with 0.452, 0.537, and 0.410 F_1 scores (Table 1), respectively (right three examples in the last row in Figure 3). The histogram of helix F_1 scores suggests that below an F_1 score of 0.55, there is a poor map/model similarity of helices.

An averaged F_1 score was calculated at a chain level to represent the overall density fitting at multiple helices in a chain. In some chains, it is possible to have helices with different levels of cylindrical similarity. As an example, in Chain 2 of PDB ID 5ln3, the density regions at five helices have F_1 scores of 0.761, 0.769 (green in Figure 1), 0.631, 0.700 (orange in Figure 1), and 0.567 (red in Figure 1), respectively. The F_1 score of a chain was calculated as a weighted average of F_1 scores of all helices, in which the weights were derived by the lengths of helices. Similar asymmetric distribution of F_1 scores between the left and the right side of the most popular F_1 scores was also observed at the chain level. The most popular score for a chain was between 0.54 and 0.56 (Figure 3B). The results suggest that chains with F_1 scores lower than 0.54 exhibited poor similarity. The scores at the helix level varied greatly, with minimum and maximum F_1 scores of 0.171 and 0.848, respectively.

The F_1 scores are agnostic of the origin of dissimilarities; both errors in maps and in models can lower the score. To compare with another established local measure, we created local resolution maps using the *MonoRes* tool[37] for the 20 helices that were analyzed using cylindrical similarity (shown in Figure 3). *MonoRes* focuses exclusively on the map quality, and not on the atomic model, so we did not necessarily expect similar results.

To visualize local resolutions in the vicinity of a helix, density regions were extracted using 7 Å radial distance from the central axis determined by *AxisComparison*. *MonoRes* produced local resolutions for 18 of the 20 EMDB map entries. All 18 cases were displayed at the density thresholds that maximize the F_1 score in each case. Although local resolution and cylindrical similarity measure different properties at different levels of detail, the two scores share certain similarities. We observed that the best F_1 scores were often associated with more uniform local resolutions at the helix region. The five highest F_1 scores of the 18 cases (top row in Figure 5) had F_1 scores between 0.741 and 0.863. The density at the five helix regions had similar local resolutions of about 5 Å to 7.5 Å (darker blue to light blue in Figure 5). This suggests that helices with the best F_1 scores tended to have similar local resolutions near the high end of the medium-resolution range. We also observed that high F_1 scores were not always associated with high local resolutions. For example, EMDB ID 2605

chain S (second example of the second row in Figure 5) had a good cylindrically shaped density, with an F_1 score of 0.717, whereas voxels on the surface showed about 9 Å resolution (Figure 5). This suggests that cylindrical helix density can be detected accurately in good quality cryo-EM maps, even near the low end of the medium-resolution range. The two cases with the lowest F_1 scores (right two on the bottom row of Figure 5) had missing density regions and hence were weak in cylindrical character. For the helix in EMDB ID 1440, which had an F_1 score of 0.410, many voxels on the surface exhibited low-resolution values of about 10 Å (Figure 5). In the case of the helix in EMDB ID 4324, the F_1 score was 0.452, and voxels with resolutions of about 6 and 10 Å were observed.

The F_1 score measures the cylindrical similarity between the density and the model at a helix region. This is reflected in the results, showing that the highest scoring densities, such as the top 5 (row 1 in Figure 5), were cylindrical in shape and associated with higher local resolution that is also spatially homogeneous. Those with lower F_1 scores deviated from a cylinder shape and were mostly associated with lower or spatially fluctuating local resolution. F_1 scores collectively compare the density with the model of a helix. Local resolution varies from voxel to voxel, and for poor similarity map/model pairs, we observed that there could be as much as a 5 Å difference in local resolution within the same helix region.

DISCUSSION AND CONCLUSIONS

Quantifying the local fit at the secondary structure level is important for validating medium- (5–10 Å) resolution density maps and their associated atomic models. Earlier local measures focused mainly on the amino acid residue level, which is applicable to higher resolutions at which side chain densities are distinguishable.[31,32] The CC score between the experimental map and a simulated map (based on the model) or the map value at specific side chain atoms was used in earlier work.[31–33] It is more challenging to measure the local fit in medium-resolution maps, since density features at the secondary structure level are less reliable than individual atoms. The proposed F_1 score method is a shape-based geometric measure that does not use CC, and hence it avoids the challenge of producing a realistic expected density map for secondary structures. It also ignores minor differences in side chain appearance and focuses on the shape of a helix backbone that resembles a cylinder. This idea is based on our experience that side chain features are not distinguishable at medium resolution.

Cryo-EM density maps at medium resolution provide significant challenges for interpretation. With a growing number of atomic models derived from such density maps, using both template structures and fitting, it is important to understand how well models fit in reliable density regions of such maps. Since helices often show as cylindrical density in medium resolutions, we proposed a measure of cylindrical similarity for each helix using the natural shape of a helix backbone. The proposed method was applied to 30,994 helices in medium-resolution density maps and shown to be effective in distinguishing different levels of cylindrical similarity. The best F_1 scores tended to be associated with spatially uniform local resolution of about 5 Å to 7.5 Å. Due to its discriminating power, the F_1 score is a potential optimization criterion for the local fitting and refinement of an atomic model at a helix for medium-resolution maps.

In this paper, the F_1 similarity score was designed to be agnostic of the origin of a specific structural mismatch (regions ExMod or ExDen in Figure 2C). This simple design of our score is both an advantage and a limitation. It is an advantage because the measure can be used to quickly extract good matching map/model pairs from the EMDB database without being concerned about lower scoring cases. It is a limitation because, at present, we do not distinguish between regions ExMod or ExDen in Figure 2C for lower levels of similarity (although our *Pden* and *Rmod* accuracies in eqs 2 and 3 could provide such a differentiation in future work).

Without knowing the ground truth, it is often difficult to speculate whether density or model is more correct in the lower-scoring cases. For example, algorithmic or conceptual limitations, such as imprecise local refinement or flexible fitting and the use of a global fitting criterion, can place helix fragments into densities that do not support the placement (ExMod). However, heterogeneity of the biomolecular structure, flexibility, or libration of the specimen could conspire to reduce alignment of corresponding image intensities such that an aggressively modeled helix might be more accurate than the weak cryo-EM density in that region. Since models are created with very diverse algorithmic approaches, it is unlikely that a single criterion will do justice to all lower-scoring map/model pairs. However, a low F_1 score could be a starting point for further study of pathological cases detected by it.

Funding

The work in this paper was supported by NSF DBI-1356621 and NIH R01-GM062968.

REFERENCES

(1). Berman HM; Westbrook J; Feng Z; Gilliland G; Bhat TN; Weissig H; Shindyalov IN; Bourne PE The Protein Data Bank. Nucleic acids research 2000, 28, 235–42. [PubMed: 10592235]

(2). Lawson CL; Baker ML; Best C; Bi C; Dougherty M; Feng P; van Ginkel G; Devkota B; Lagerstedt I; Ludtke SJ; Newman RH; Oldfield TJ; Rees I; Sahni G; Sala R; Velankar S; Warren J; Westbrook JD; Henrick K; Kleywegt GJ; Berman HM; Chiu W EMDataBank.org: unified data resource for CryoEM. Nucleic Acids Res. 2011, 39, D456–D464. [PubMed: 20935055]

(3). Pettersen EF; Goddard TD; Huang CC; Couch GS; Greenblatt DM; Meng EC; Ferrin TE UCSF Chimera–a visualization system for exploratory research and analysis. J. Comput. Chem 2004, 25, 1605–12. [PubMed: 15264254]

(4). Emsley P; Lohkamp B; Scott WG; Cowtan K Features and development of Coot. Acta Crystallogr., Sect. D: Biol. Crystallogr 2010, 66, 486–501. [PubMed: 20383002]

(5). Afonine PV; Poon BK; Read RJ; Sobolev OV; Terwilliger TC; Urzhumtsev A; Adams PD Real-space refinement in PHENIX for cryo-EM and crystallography. Acta Crystallographica Section D 2018, 74, 531–544.

(6). McCallum M; Benlekbir S; Nguyen S; Tammam S; Rubinstein JL; Burrows LL; Howell PL Multiple conformations facilitate PilT function in the type IV pilus. Nat. Commun 2019, 10, 5198. [PubMed: 31729381]

(7). Vinothkumar KR; Montgomery MG; Liu S; Walker JE Structure of the mitochondrial ATP synthase from Pichia angusta determined by electron cryo-microscopy. Proc. Natl. Acad. Sci. U. S. A 2016, 113, 12709–12714. [PubMed: 27791192]

(8). Letts JA; Fiedorczuk K; Sazanov LA The architecture of respiratory supercomplexes. Nature 2016, 537, 644–648. [PubMed: 27654913]

(9). Xu J; Lahiri I; Wang W; Wier A; Cianfrocco MA; Chong J; Hare AA; Dervan PB; DiMaio F; Leschziner AE; Wang D Structural basis for the initiation of eukaryotic transcription-coupled DNA repair. Nature 2017, 551, 653–657. [PubMed: 29168508]

(10). Song Y; DiMaio F; Wang RY-R; Kim D; Miles C; Brunette TJ; Thompson J; Baker D High-Resolution Comparative Modeling with RosettaCM. Structure 2013, 21, 1735–1742. [PubMed: 24035711]

(11). Wehmer M; Rudack T; Beck F; Aufderheide A; Pfeifer G; Plitzko JM; Forster F; Schulten K; Baumeister W; Sakata E Structural insights into the functional cycle of the ATPase module of the 26S proteasome. Proc. Natl. Acad. Sci. U. S. A 2017, 114, 1305–1310. [PubMed: 28115689]

(12). Sali A; Blundell TL Comparative protein modelling by satisfaction of spatial restraints. J. Mol. Biol 1993, 234, 779–815. [PubMed: 8254673]

(13). Trabuco LG; Villa E; Mitra K; Frank J; Schulten K Flexible fitting of atomic structures into electron microscopy maps using molecular dynamics. Structure (Oxford, U. K.) 2008, 16, 673–683.

(14). Trabuco LG; Villa E; Schreiner E; Harrison CB; Schulten K Molecular dynamics flexible fitting: A practical guide to combine cryo-electron microscopy and X-ray crystallography. Methods 2009, 49, 174–180. [PubMed: 19398010]

(15). Chapman MS Restrained real-space macromolecular atomic refinement using a new resolution-dependent electron-density function. Acta Crystallogr., Sect. A: Found. Crystallogr 1995, 51, 69–80.

(16). Chen LF; Blanc E; Chapman MS; Taylor KA Real Space Refinement of Acto-myosin Structures from Sectioned Muscle. J. Struct. Biol 2001, 133, 221–232. [PubMed: 11472093]

(17). Wriggers W; Agrawal RK; Drew DL; McCammon A; Frank J Domain Motions of EF-G Bound to the 70S Ribosome: Insights from a Hand-Shaking between Multi-Resolution Structures. Biophys. J 2000, 79, 1670–1678. [PubMed: 10969026]

(18). Wriggers W; Birmanns S Using Situs for Flexible and Rigid-Body Fitting of Multiresolution Single-Molecule Data. J. Struct. Biol 2001, 133, 193–202. [PubMed: 11472090]

(19). Jiang W; Baker ML; Ludtke SJ; Chiu W Bridging the information gap: computational tools for intermediate resolution structure interpretation. J. Mol. Biol 2001, 308, 1033–44. [PubMed: 11352589]

(20). Kong Y; Ma J A structural-informatics approach for mining beta-sheets: locating sheets in intermediate-resolution density maps. J. Mol. Biol 2003, 332, 399–413. [PubMed: 12948490]

(21). Dal Palu A; He J; Pontelli E; Lu Y Identification of Alpha-Helices from Low Resolution Protein Density Maps. Proceeding of Computational Systems Bioinformatics Conference(CSB) 2006, 89–98.

(22). Baker ML; Ju T; Chiu W Identification of secondary structure elements in intermediate-resolution density maps. Structure 2007, 15, 7–19. [PubMed: 17223528]

(23). Yu Z; Bajaj C Computational Approaches for Automatic Structural Analysis of Large Biomolecular Complexes. IEEE/ACM Trans. Comput. Biol. Bioinf 2008, 5, 568–582.

(24). Rusu M; Wriggers W Evolutionary bidirectional expansion for the tracing of alpha helices in cryo-electron microscopy reconstructions. J. Struct. Biol 2012, 177, 410–9. [PubMed: 22155667]

(25). Si D; Ji S; Al Nasr K; He J A machine learning approach for the identification of protein secondary structure elements from electron cryo-microscopy density maps. Biopolymers 2012, 97, 698–708. [PubMed: 22696406]

(26). Si D; He J In Proceedings of the International Conference on Bioinformatics, Computational Biology and Biomedical Informatics; ACM: Washington, DC, USA, 2013; pp 764–770, DOI: 10.1145/2506583.2506707.

(27). Wriggers W; He J Numerical geometry of map and model assessment. J. Struct. Biol 2015, 192, 255–261. [PubMed: 26416532]

(28). Kucukelbir A; Sigworth FJ; Tagare HD Quantifying the local resolution of cryo-EM density maps. Nat. Methods 2014, 11, 63–65. [PubMed: 24213166]

(29). Vilas JL; Gómez-Blanco J; Conesa P; Melero R; Miguel de la Rosa-Trevín J; Otón J; Cuenca J; Marabini R; Carazo JM; Vargas J; Sorzano COS MonoRes: Automatic and Accurate Estimation

of Local Resolution for Electron Microscopy Maps. Structure 2018, 26, 337–344 e4. [PubMed: 29395788]

(30). Wriggers W Conventions and workflows for using Situs. Acta Crystallogr., Sect. D: Biol. Crystallogr 2012, 68, 344–351. [PubMed: 22505255]

(31). Afonine PV; Klaholz BP; Moriarty NW; Poon BK; Sobolev OV; Terwilliger TC; Adams PD; Urzhumtsev A New tools for the analysis and validation of cryo-EM maps and atomic models. Acta Crystallogr. D Struct Biol 2018, 74, 814–840. [PubMed: 30198894]

(32). Barad BA; Echols N; Wang RY; Cheng Y; DiMaio F; Adams PD; Fraser JS EMRinger: side chain-directed model and map validation for 3D cryo-electron microscopy. Nat. Methods 2015, 12, 943–6. [PubMed: 26280328]

(33). Pintilie G; Chiu W Assessment of structural features in Cryo-EM density maps using SSE and side chain Z-scores. J. Struct. Biol 2018, 204, 564–571. [PubMed: 30144506]

(34). Zeil S; Kovacs J; Wriggers W; He J Comparing an Atomic Model or Structure to a Corresponding Cryo-electron Microscopy Image at the Central Axis of a Helix. Journal of Computational Biology 2017, 24, 52–67. [PubMed: 27936925]

(35). Haslam D; Sazzed S; Wriggers W; Kovacs J; Song J; Auer M; He J A Pattern Recognition Tool for Medium-Resolution Cryo-EM Density Maps and Low-Resolution Cryo-ET Density Maps. In Bioinformatics Research and Applications; Zhang F, Cai Z, Skums P, Zhang S, Eds.; Springer International Publishing: Cham, 2018; pp 233–238, DOI: 10.1007/978-3-319-94968-0_22.

(36). Van Rijsbergen CJ Information Retrieval, 2nd ed.; Butterworth-Heinemann: 1979.

(37). de la Rosa-Trevin JM; Quintana A; Del Cano L; Zaldivar A; Foche I; Gutierrez J; Gomez-Blanco J; Burguet-Castell J; Cuenca-Alba J; Abrishami V; Vargas J; Oton J; Sharov G; Vilas JL; Navas J; Conesa P; Kazemi M; Marabini R; Sorzano CO; Carazo JM Scipion: A software framework toward integration, reproducibility and validation in 3D electron microscopy. J. Struct. Biol 2016, 195, 93–9. [PubMed: 27108186]

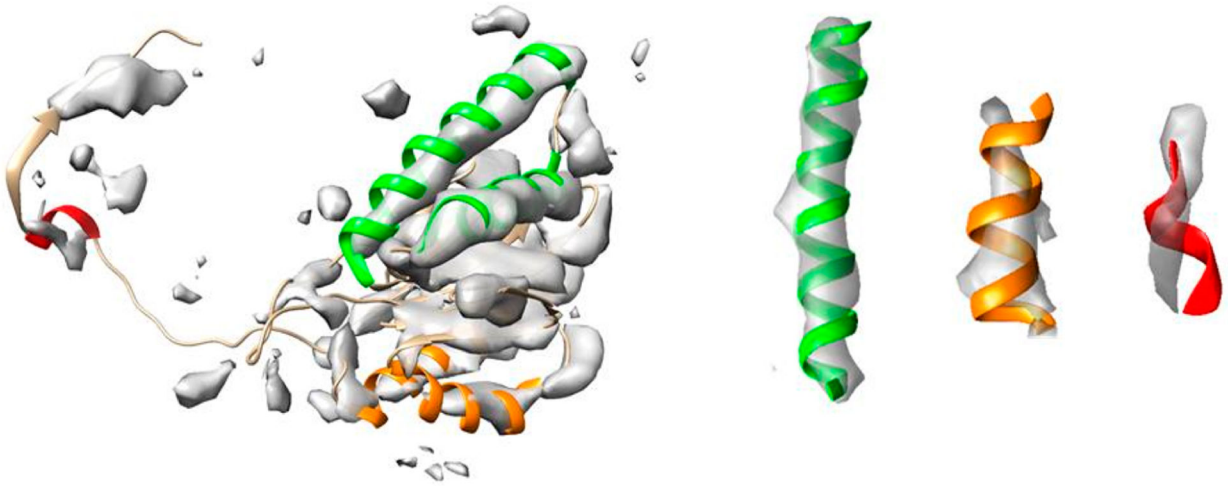

Figure 1.

Illustration of different levels of map/model similarity exhibited by helices in the same map. The surface representation of the density map (EMDB ID 4089, gray, corresponding to Chain 2) is superimposed on Protein Data Bank (PDB) ID 5ln3 Chain 2 (ribbon). Helices with different levels of similarity are indicated by green, orange, and red, respectively, from strong similarity to poor similarity (with separate views, on the right, for three examples). For detailed F_1 similarity scores, see the Results section.

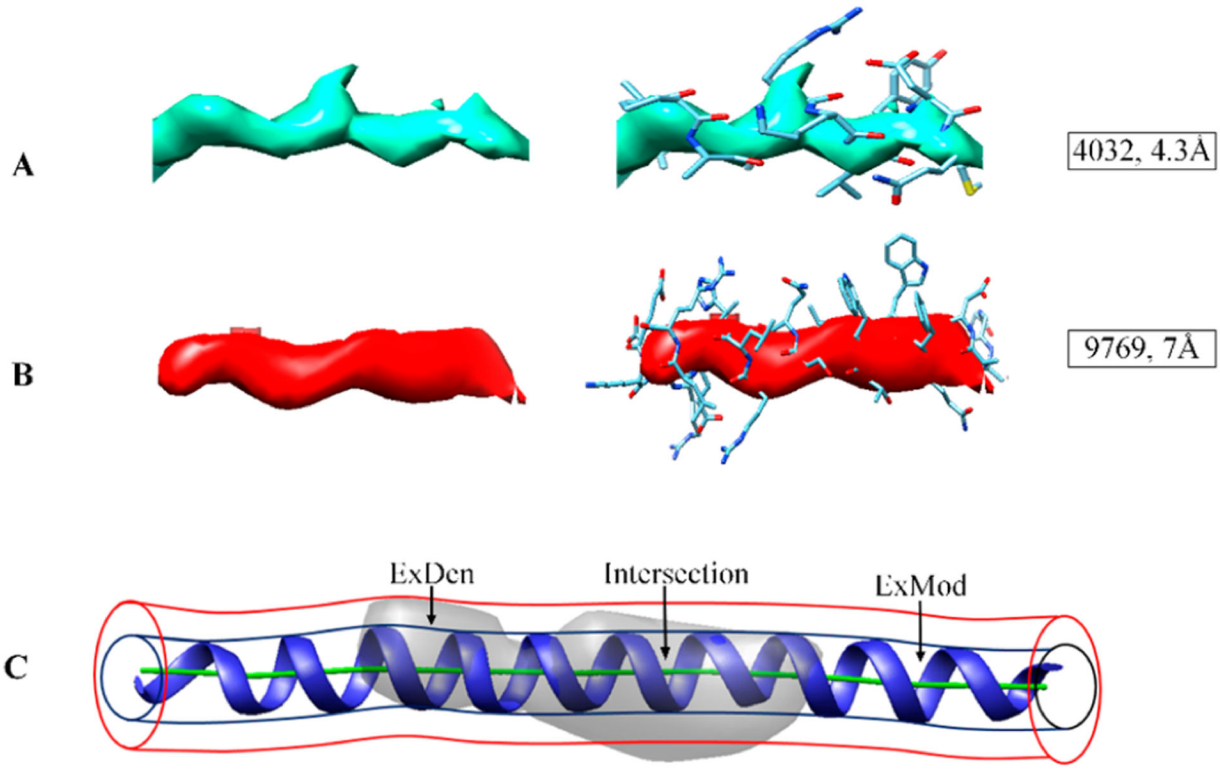

Figure 2.

Examples of helix densities at different resolutions and their cylindrical similarity: (A) density for a helix in EMDB ID 4032 with 4.3 Å resolution superimposed on the atomic model; (B) density for a helix in EMDB ID 9769 with 7 Å resolution superimposed on the atomic model; (C) two template cylinders of 2.5 and 4 Å radii, respectively, were used to measure the cylindrical similarity (see section “Cylindrical Similarity Score”). Part (C) shows the intersection of map and model and two mismatched regions, ExDen and ExMod (where density is not accounted for by the model or vice versa).

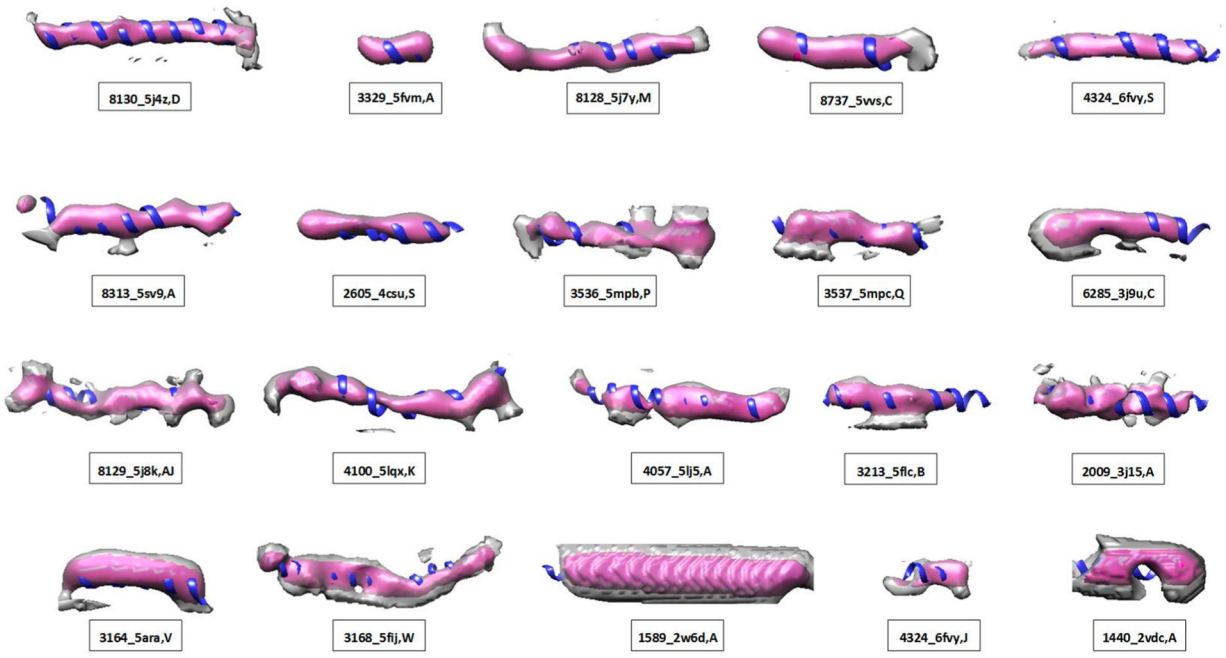

Figure 3.

Twenty examples of helical map/model pairs with F_1 similarity scores (see Table 1). The atomic structure of a helix (ribbon) is superimposed on the density extracted using 4 Å radius (pink) and 7 Å radius (gray, to visualize the immediate neighborhood), respectively, around the central axis of the helix. Each helix density is displayed using the threshold that optimizes the F_1 score. Panels are sorted by the F_1 score from top left to lower right (see details in Table 1).

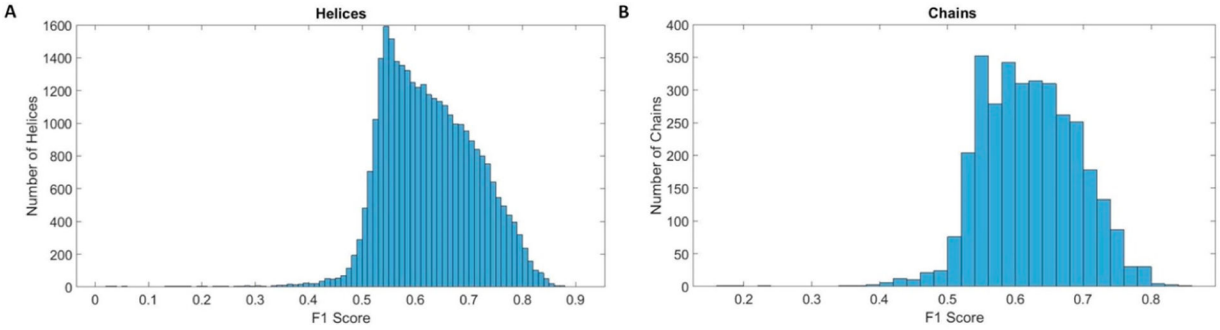

Figure 4.

Histograms of F_1 scores in medium-resolution maps: (A) the histograms of F_1 scores for 30,994 helices and (B) the histograms of F_1 scores for 3,247 protein chains.

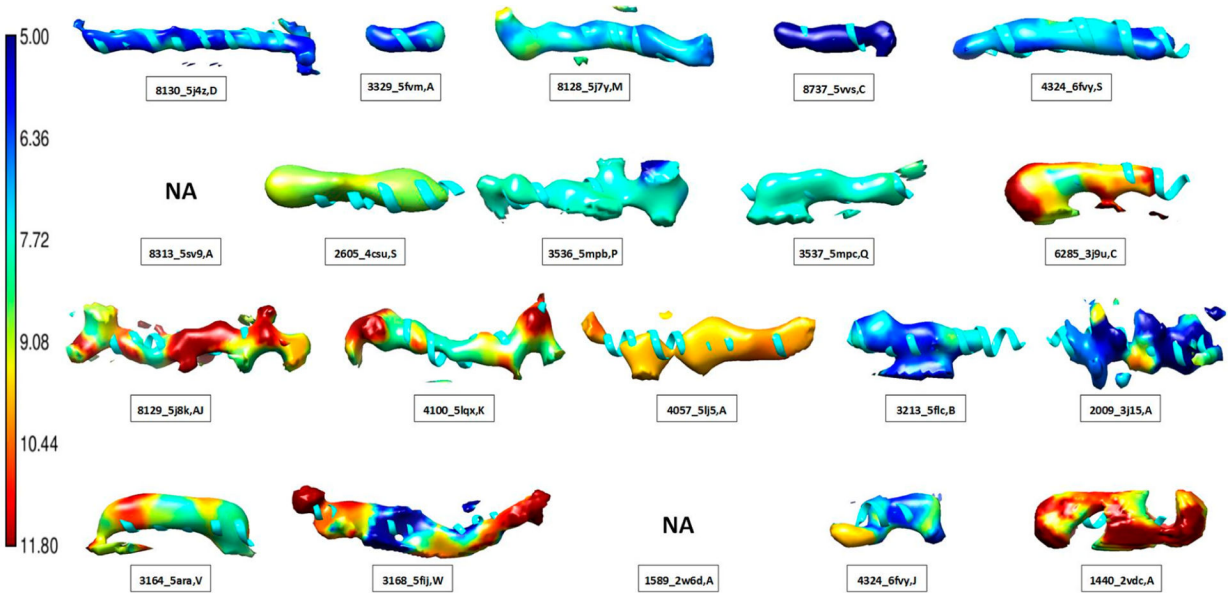

Figure 5.

Local resolution of 18 helix regions. Density regions near helices were extracted using a cylinder of 7 Å in radius from the central axis of the corresponding helix model (ribbon). Local resolutions produced using *MonoRes*[29] were used to color the density according to the resolution bar (left). The EMDB ID, PDB ID, and chain ID are provided for each helix. Refer to Table 1 for their amino acid segment and the F_1 score in each case. The threshold that maximizes the F_1 score was used in displaying density. Panels are sorted by the F_1 score such that the upper-left helix has the highest F_1 score and the lower-right has the lowest.

Table 1.

Various Levels of Cylindrical Similarity Evaluated by Their F_1 Scores for 20 Helices[a]

ID[A]	Ch[B]	segment	F_1	P[C]	R[D]	T[E]	res[F]
8130_5j4z	D	131–161	0.863	0.863	0.863	0.159	5.8
3329_5fvm	A	884–891	0.833	0.851	0.817	0.129	6.7
8128_5j7y	M	63–85	0.794	0.75	0.845	0.137	6.7
8737_5vvs	C	26–39	0.751	0.741	0.76	0.039	6.4
4324_6fvy	S	306–325	0.741	0.817	0.678	0.03	6.1
8313_5sv9	A	161–188	0.738	0.769	0.709	165.048	5.9
2605_4csu	S	43–60	0.717	0.696	0.739	0.105	5.5
3536_5mpb	P	334–356	0.698	0.613	0.809	0.039	7.8
3537_5mpc	Q	253–273	0.688	0.681	0.695	0.046	7.7
6285_3j9u	C	597–616	0.675	0.625	0.734	0.036	7.6
8129_5j8k	AJ	16–47	0.668	0.574	0.797	0.096	7.8
4100_5lqx	K	46–75	0.662	0.592	0.75	0.147	7.9
4057_5lj5	A	841–870	0.646	0.591	0.712	0.035	10
3213_5flc	B	1736–1762	0.632	0.658	0.608	0.085	5.9
2009_3j15	A	176–198	0.621	0.604	0.64	0.132	6.6
3164_5ara	V	29–47	0.618	0.515	0.774	0.192	7.4
3168_5fij	W	138–182	0.597	0.465	0.831	0.159	7.4
1589_2w6d	A	5–44	0.537	0.392	0.854	0.243	9
4324_6fvy	J	131–141	0.452	0.365	0.592	0	6.1
1440_2vdc	A	619–633	0.41	0.326	0.553	35.314	9.5

[a]See Figure 3. Columns from left to right are (A) EMDB ID, PDB ID; (B) chain ID, amino acid segment of the helix, the best F_1 score; (C) *Pden*, the accuracy of helix density; (D) *Rmod*, the accuracy of helix backbone model; (E) the density threshold that maximizes the F_1 score; and (F) resolution of the density map.